

Cell Structure of 2D Cohesive Granular Solid

Takashi Matsushima^{1,*}, Zhipeng Yu¹, Dominik Krenzel², and Raphael Blumenfeld³

¹ Department of Engineering Mechanics and Energy, University of Tsukuba, Tsukuba, 305-8573, JAPAN

² Department of Marine Resources and Energy, Tokyo University of Marine Science, Tokyo, 108-8477, JAPAN

³ Gonville & Caius College, University of Cambridge, Trinity Street, Cambridge CB2 1TA, UK

Abstract. This study presents an analysis of granular cell, defined by the smallest loop of grains in contact, observed in 2D cohesive granular materials using Discrete Element simulations. The adopted particle interaction is the combination of non-contact DLVO force and linear contact repulsion. 9000 mono-sized disk particles were randomly generated in a double-periodic space with a very loose unjammed state, and then compressed isotropically to keep its uniformity by equilibrating the external isotropic compressive stress with agglomeration stress. The external stress was increased stepwise to reproduce the oedometer test in soil mechanics. Then we investigated the granular cell statistics for each loading step. What we found is the following: (1) Within the examined pressure range, the $e - \log p$ curve can be well approximated by a straight line, and the effect of interparticle friction appears to be negligible. However, the mean coordination number \bar{z} shows a clear dependence on interparticle friction. (2) The distribution of cell volumes transitions from a power-law to an exponential form as the external load increases. This suggests that the larger cells are mechanically weaker and tend to collapse earlier. (3) The average cell shape becomes more circular with increasing external load, indicating that circular cells are more stable under compressive stress than elongated ones. Those results suggest that the granular cell approach is also applicable and effective for analysing cohesive granular systems.

1 Introduction

The granular cell structure is defined as the smallest closed loop of grains in contact in a granular system. It has been extensively studied in cohesionless granular solids over the past decades, primarily through numerical simulations using the Discrete Element Method (DEM) [1-5]. Unlike the ‘force chain’ structure, a granular cell is considered an elementary structural unit in granular solids, within which stress and strain can be clearly defined. Therefore, it is regarded as a promising meso-structural element for bridging grain-scale mechanics and bulk behaviour.

Recently, Matsushima and Blumenfeld [6] as well as Jiang et al. [7], defined cell stress in a two-dimensional cohesionless granular solid under compression. They demonstrated that the cell stress ratio, $h = q/p$ - where p and q are the mean and deviatoric cell stresses, respectively - follows a unique probability density function that is well described by the Weibull distribution. Furthermore, the normalized distribution $P(h/\bar{h})$ collapses onto a single curve regardless of the initial packing condition or interparticle friction. They also found that the principal direction of stress statistically coincides with the long axis of the cell. These intriguing features strongly suggest that the granular cell plays a key mechanical role in bridging the particle scale with the bulk continuum scale.

This study extends such granular cell analysis to

systems of cohesive particles under compression using two-dimensional DEM. Cohesive particle systems are defined as those in which interparticle adhesive forces are sufficiently large compared to body forces or external loads. Similar simulations have been widely employed in studies of the compressive behaviour of clays in geotechnical engineering [8-10], while Gilibert et al. [11] made pioneering contributions to granular physics by characterizing packing structures using dimensionless parameters. In contrast to previous studies, our cell analysis has shed new light on the packing structure of cohesive granular materials.

2 Simulation overview

The particle interaction model used in this study is the combination of non-contact DLVO force and linear contact repulsion, as illustrated in Figure 1. The DLVO

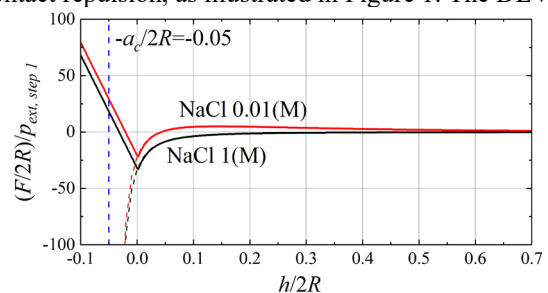


Fig. 1. Normalized interaction force as a function of normalized particle separation

* Corresponding author: tmatsu@kz.tsukuba.ac.jp

force is computed by the following potential:

$$U = -\frac{AR}{12h} + \frac{2\pi R\rho_c^2}{\kappa^2\varepsilon} \exp(-\kappa h) \quad (1)$$

where h is the surface separation between particles, A is the Hamaker constant, and R is particle radius. A is set to the value of mica/water/mica in this study [12]. For the electrostatic double layer (EDL) parameters, σ is the surface charge density, ε is the permittivity of the medium (water). κ is the inverse Debye length. The DLVO parameters used in this study are summarized in Table 1.

Under these conditions, the DLVO potential does not exhibit an energy barrier, allowing two particles to approach each other until contact. To avoid the divergence of attractive forces as $h \rightarrow 0$, we replace h with $h - a_c$ in Fig.1, in which $a_c=0.5(\text{nm})$, known as the minimum separation [9, 13]. At this point, the net pairwise forces transitions to a contact force calculated using the standard linear spring-dashpot-slider model, following previous studies [9, 13]. The interparticle friction coefficient μ is set to either 0.5 or 10 to investigate its influence on the packing structure. The linear contact model parameters are summarized in Table 2. The particle density is fixed at $\rho_s=1.5(\text{g/cm}^3)$.

9000 mono-sized disk particles were randomly generated in a double-periodic domain in an initially very loose, unjammed state. The system was then isotropically compressed to maintain uniformity by balancing the external isotropic compressive stress, p_{ext} , with the agglomeration stress. The external stress was increased stepwise to simulate an oedometer test, as commonly used in soil mechanics.

Figure 2 shows the relationship between the external pressure and the resulting void ratio at each equilibrated state, commonly referred to as the $e - \log p$ curve. Within the examined pressure range, the curve can be well approximated by a straight line, and the effect of interparticle friction appears to be negligible.

Figure 3 illustrates the packing structures at each step for the case of $\mu=0.5$. The red lines represent contact forces, with line thickness proportional to the force magnitude. It is clearly observed that larger voids present in the early stages progressively collapse and disappear in the later stages.

In contrast to Figure 2, the evolution of the mean

Table 1. DLVO parameters used in the simulation

| Parameter | Value |
|---|---|
| Particle radius, R | 5.0 (nm) |
| Hamaker constant, A | 2.0×10^{-20} (J) |
| Surface density of charge, ρ_c | 0.01 (C/m ²) |
| Dielectric constant of water, ε | $80 \times 8.85 \times 10^{-12}$ (s ⁴ A ² /m ³ kg) |
| Debye length, $1/\kappa$ | 0.304 (nm) NaCl 1(M) |

Table 2. Linear contact model parameters

| Parameter | Value |
|---------------------------------|------------------------------|
| Spring constant, k_n, k_s | 0.1 (N/m) |
| Damping coefficient, c_n, c_s | 1.0×10^{-8} (N s/m) |
| Friction coefficient, μ | 0.5, 10 |

coordination number of the system \bar{z} at each loading step in Figure 4 exhibits a clear dependence of interparticle friction. The inset provides a close-up view of a packing structure, showing that particles form stable, column-like arrangements. The stability of these structures under external compressive stress depends on both the magnitude of attractive force and friction, with more contact points required in cases of lower friction.

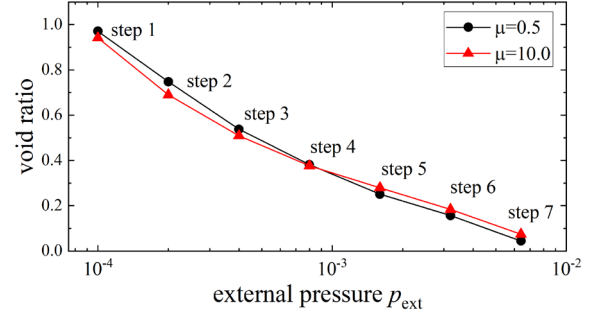


Fig. 2. $e - \log p$ curves in the oedometer simulation

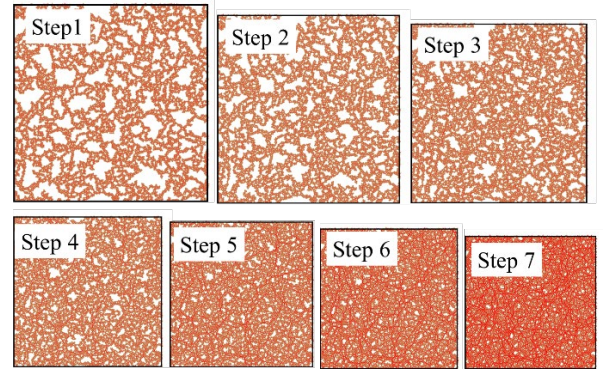


Fig. 3. Packing structures at each step for the specimen with $\mu=0.5$. Red lines represent contact forces.

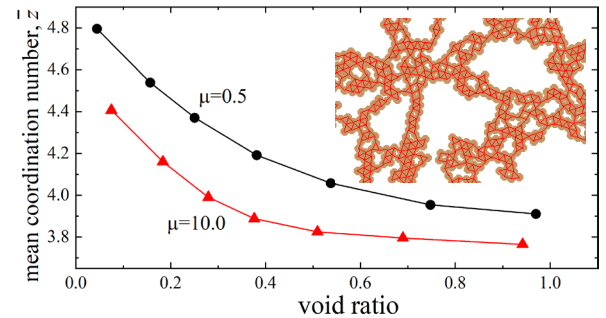


Fig. 4. Evolution of the mean coordination number \bar{z} as a function of void ratio

3 Granular cell analysis

In two-dimensional disc systems, a granular cell is defined as the smallest (irreducible) closed loop of disc centres surrounding a void. Under this definition, the total volume of the system is equivalent to the sum of all cell volumes. From Euler's topological relation, the following relationship between the mean cell order \bar{c} and the mean coordination number \bar{z} can be derived for a sufficiently large system [14,15]:

$$\bar{c} = \frac{2\bar{z}}{\bar{z} - 2} \quad (2)$$

Figure 5 demonstrates that this relationship holds at every loading step regardless of the interparticle friction.

Figure 6 illustrates examples of cell structures at Step 1 and Step 7 for the case of $\mu = 0.5$. A considerable number of triangular cells are observed in both steps due to the presence of interparticle attraction. In Step 1, these triangular cells are interconnected to form column-like structures, which allow even relatively large cells remain stable. In Step 7, by contrast, such large cells are no longer present, as they cannot withstand the increased external pressure - only smaller cells persist.

This mechanism of cell “survival” is analogous to the grain crushing process described in [16], in which (1) the crushing stress increases as grain size decreases, and (2) larger grains become stable when they are surrounded by smaller grains. Accordingly, the probability density function (PDF) of cell size is also expected to follow a power-law (or fractal) distribution. Figures 7 and 8 present the frequency distributions of the cell order c and the cell volume v_c normalized by the particle volume v_g , for the specimen with $\mu=0.5$. The latter appears linear in log-log plot, indicating a power law distribution with an exponent close to two.

It should be noted, however, that this power law behaviour gradually shifts towards something like an exponential distribution in the final loading steps, similar to what has been observed in cohesionless particle systems [14,15], as the external pressure becomes sufficiently large compared to the interparticle attraction.

To clarify the differing trends observed in Figures 7 and 8, the relationship between the cell order c and the normalized cell volume v_c/v_g for each cell at every

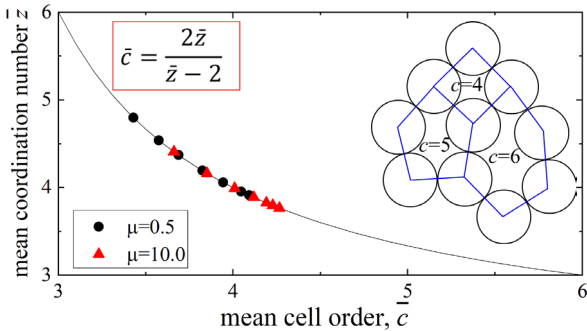


Fig. 5. Relationship between the mean cell order \bar{c} and the mean coordination number \bar{z} at each loading step for specimens with $\mu=0.5$ and $\mu=10.0$

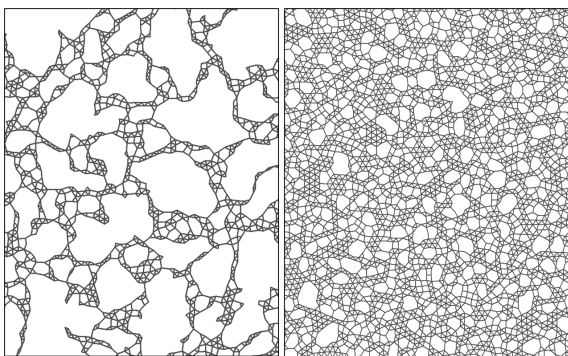


Fig. 6. Cell structure for step 1 (left) and step 7 (right) for the specimen with $\mu=0.5$

loading step is plotted in Figure 9. The deviations observed in the scatter are attributed to differences in cell shape. Extending the analysis by Matsushima and Blumenfeld [6,15] for cohesionless particle systems, cell shape is approximated by an elliptical polygon with varying aspect ratio b/a , where a and b denote the major and minor axes of the ellipse, respectively. The model predictions are shown in the figure as dashed lines. The observed trend can be explained by the elliptical polygon model for cells with lower cell order, while larger cells deviate from this trend. This discrepancy is due to the jagged (non-smooth) geometry of actual larger cells, which cannot be well approximated by ellipses, as shown in Figure 10. This implies the necessity to consider a higher order shape indicator to model it.

Despite this discrepancy, the histogram of the cell aspect ratio b/a still exhibit a systematic trend: it increases with increasing external pressure, as shown in Figure 11. This trend is more clearly demonstrated in Figure 12, which presents the average aspect ratio $\langle b/a \rangle$ as a function of external pressure. This can also be interpreted in terms of cell stability – namely, elongated cells become less stable as they grow larger.

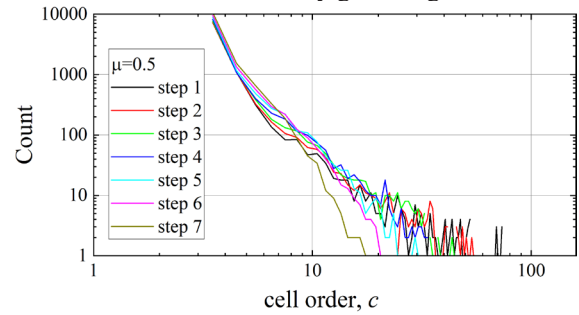


Fig. 7. Evolution of frequency distribution of cell order c for the specimen with $\mu=0.5$

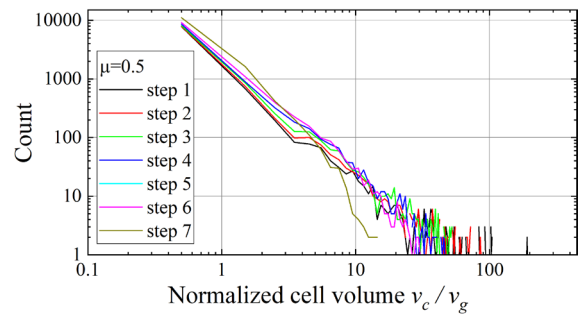


Fig. 8. Evolution of frequency distribution of normalized cell volume for the specimen with $\mu=0.5$

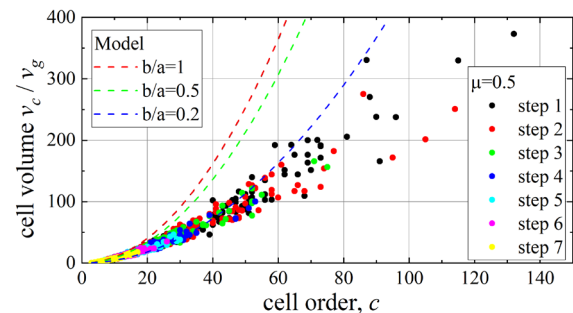


Fig. 9. Relationship between cell order c and normalized cell volume v_c/v_g for each cell for the specimen with $\mu=0.5$

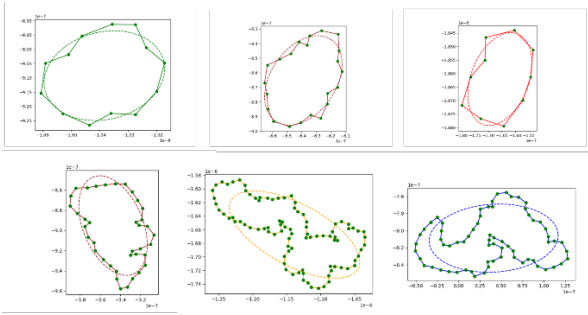


Fig. 10. Examples of actual cells from the simulated system and their corresponding elliptical approximations

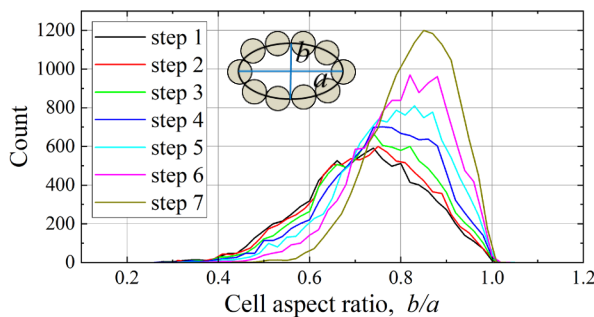


Fig. 11. Evolution of frequency distribution of cell aspect ratio b/a for the specimen with $\mu=0.5$

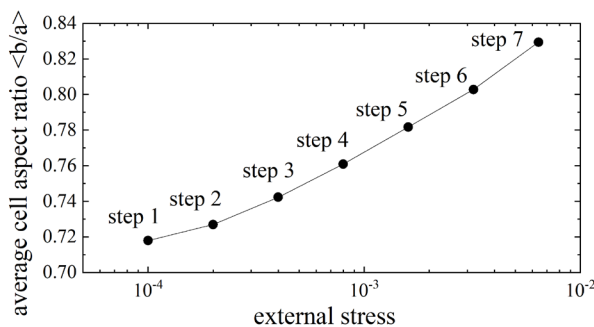


Fig. 12. Average aspect ratio $\langle b/a \rangle$ as a function of external pressure for the specimen with $\mu=0.5$

4 Conclusion

A series of two-dimensional discrete element method (DEM) simulations of isotropic compression for cohesive particles was conducted to investigate the evolution of the geometrical properties of granular cells. The key findings are summarized as follows.

(1) Within the examined pressure range, the $e - \log p$ curve can be well approximated by a straight line, and the effect of interparticle friction appears to be negligible. However, the mean coordination number \bar{z} shows a clear dependence on interparticle friction.

(2) The distribution of cell volumes transitions from a power-law to an exponential form as the external load increases. This suggests that the larger cells are mechanically weaker and tend to collapse earlier.

(3) The average cell shape becomes more circular with increasing external load, indicating that circular cells are more stable under compressive stress than elongated ones.

It should be emphasized that cell volume is a critical micro-variable for evaluating the bulk void ratio of the system. The above findings demonstrate that not only the cell order but also the cell shape must be considered to develop a micromechanics-based compression model.

Furthermore, snapshots of the cell structure revealed that larger cells are often stabilized by the support of surrounding smaller cells. This suggests that spatial correlation in cell size play a significant role and should not be neglected – an aspect that will be explored in future work.

Overall, the results of this study suggest that the granular cell approach is also applicable and effective for analysing cohesive granular systems.

This work was supported by JSPS KAKENHI Grant Number 21KK0071 and 21H01422.

References

1. Ball, R.C. and Blumenfeld, R., 2002. *Physical review letters*, 88(11), p.115505.
2. Tordesillas, A., Lin, Q., Zhang, J., Behringer, R.P. and Shi, J., 2011. *Journal of the Mechanics and Physics of Solids*, 59(2), pp.265-296.
3. Kuhn, M.R., 2014. *Granular Matter*, 16(4), pp.499-508.
4. Wan, R. and Pouragha, M., 2015. *Continuum Mechanics and Thermodynamics*, 27, pp.243-259.
5. Kruyt, N.P. and Rothenburg, L., 2016. *Journal of the Mechanics and Physics of Solids*, 95, pp.411-427.
6. Matsushima, T. and Blumenfeld, R., 2021. In *EPJ Web of Conferences* (Vol. 249, p. 02006). EDP Sciences.
7. Jiang, X., Blumenfeld, R. and Matsushima, T., *Physical Review E*, accepted.
8. Anandarajah, A., 1994. *Journal of Geotechnical Engineering* 120(9):1593–1613.
9. Suzuki, A and Matsushima, T., 2014. In: *Soga K et al. (eds.) Geomechanics from Micro to Macro*, pp. 33–40. Taylor & Francis, London.
10. Pagano, A.G., Magnanimo, V., Weinhart, T. and Tarantino, A., 2020. *Géotechnique* 70(4):303–316.
11. Gilabert, F.A., Roux, J.-N. and Castellanos, A., 2007. *Physical Review E*, 75, 011303.
12. Israelachvili, J.N., 2011. *Intermolecular and surface forces*. 3rd edn. Academic Press, London.
13. Yang, R. Y., R. P. Zou, and A. B. Yu, 2000. *Physical Review E* 62.3 (2000): 3900.
14. Matsushima, T. and Blumenfeld, R., 2014. *Physical review letters*, 112(9), p.098003.
15. Matsushima, T. and Blumenfeld, R., 2017. *Physical review E*, 95(3), p.032905.
16. McDowell, G.R., Bolton, M.D., 1998. *Géotechnique*, 48(5): 667-679.